CARBON 81 (2015) 731–738

Available at www.sciencedirect.com

ScienceDirect

journal homepage: www.elsevier.com/locate/carbon

Layer-by-layer scaffold formation using magnetic attraction between HiPCO® single-walled carbon nanotubes and magnetic nanoparticles: Application for high performance immunosensors

Meenakshi Singh [a,b], *Michael Holzinger* [a,*], *Maryam Tabrizian* [b], *Serge Cosnier* [a,*]

[a] *CNRS – Univ. Grenoble Alpes, DCM UMR 5250, F-38000 Grenoble, France*

[b] *McGill University, Biomat'X Research Laboratories, Dept. of Biomedical Engineering and Faculty of Dentistry, Montréal, Canada*

ARTICLE INFO

Article history:
Received 10 July 2014
Accepted 6 October 2014
Available online 12 October 2014

ABSTRACT

Iron particle impurities of HiPCO® single-walled carbon nanotubes (SWCNTs) are treated as undesirable moieties and considerable times and efforts is allocated towards research and development to reduce their amount in HiPCO® SWCNTs. Taking advantage of this impurity, 3D nanostructured scaffolds are built via layer by layer (LBL) deposition of HiPCO® SWCNTs and magnetic nanoparticles which are retained via magnetic interaction with the iron particle impurities during the scaffold formation. The resulting scaffold has an inhomogeneous structure with large vacancies that can further be reinforced by electrogeneration of a functional polymer film to enable the immobilization of bioreceptor units for biosensing. Magnetic nanoparticles of different sizes are used to adjust the pore sizes within the scaffolds in order to determine the optimal particle size for their application as highly sensitive immunosensors. Scaffolds made of the magnetic nanoparticles with in average 500 nm sizes led to a sensitivity of 88 $\mu A\ \mu g^{-1}\ mL\ cm^{-2}$ equivalent to a detection limit of 10 $ng\ mL^{-1}$ for cholera antitoxin. This is by far the highest sensitivity for anti-CT immunosensors compared to amperometric transduction or ELISA.

1. Introduction

Nanostructured electrodes for electrochemical biosensing applications is of steady increasing interest since they provide clearly enhanced specific surface for the immobilization of bioreceptor units leading to drastic improvements of these devices [1]. The design of 3D porous nanostructures that increases the density of the immobilized bioreceptor units, targets mainly the detection of small organic molecules or ions which can easily diffuse throughout these mostly mesoporous (2–50 nm) structures [2].

In the particular case of immunosensors, not only the biorecognition moieties (e.g., an antigen) have to be immobilized within these nanostructured, but also the analyte, the corresponding antibody, should have unhindered access to its corresponding antigen [3]. Furthermore, for optical or electrochemical transduction, an additional secondary antibody, labelled with a fluorescent marker or a redox enzyme

* *Corresponding authors.*
E-mail addresses: michael.holzinger@ujf-grenoble.fr (M. Holzinger), serge.cosnier@ujf-grenoble.fr (S. Cosnier).
http://dx.doi.org/10.1016/j.carbon.2014.10.015
0008-6223/

should also permeate through these structures [4]. Antigens, antibodies, and labelled secondary antibodies are biological macromolecules with over several nanometers in diameter. In the recent years, great efforts were invested to control pore sizes to extend the beneficial effect of nanostructures from enzymatic biosensing applications to immunosensors [5]. However, the construction of three-dimensional (3D) scaffolds with sufficient large pores allowing for the diffusion of all these biological compounds remains a challenge.

Beside many available nanomaterials, carbon nanotubes are considered as excellent candidates for the development of high performance bioanalytical devices due to their high conductivity and the high specific surface area [6–8]. In particular, single-walled carbon nanotubes (SWCNTs) produced by the HiPCO® process are available with almost no carbon impurities and have a relative intact π-system for efficient non-covalent functionalization [9,10]. However, these nanotubes can contain up to 15% (weight) iron catalyst particles [11] which often requires supplementary purification steps for further use of these SWCNTs [12–15]. Based on a recent study revealing magnetic properties of these iron nanoparticle impurities [16], we sought to take advantages of the undesirable presence of these catalyst particles to construct highly porous structure for immunosensing and enzymatic glucose sensing applications through magnetic interaction of these iron particles with commercial super paramagnetic nanoparticles of different sizes.

2. Experimental

2.1. Materials

Cholera toxin B subunit-biotin labeled (lyophilized powder, biotin content 1.2 mol mol^{-1} protein), peroxidase labeled IgG anti-rabbit antibody (from goat, protein content 0.8 mg mL^{-1}, affinity isolated antibody), anti-cholera toxin (from rabbit, protein content 48 mg mL^{-1}, purified toxin from *Vibriocholerae*), biotin monoclonal anti-rabbit IgG-γ-chain specific (from mouse, protein content 4.2 mg mL^{-1}), polyoxyethylene-sorbitan monolaurate (Tween® 20), bovine serum albumin (BSA), biotin-labeled glucose oxidase (GOx, 120 U mg^{-1}), glucose, hydroquinone (1,4-dihydroxy-benzene), hydrogen peroxide solution (30 wt.% in H_2O), monobasic and dibasic phosphates, 1-methyl-2-pyrrolidone (NMP) were purchased from Sigma. All chemicals were obtained commercially and used as received unless it is mentioned. Stock solutions of glucose were allowed to mutarotate at room temperature for 24 h before use, and were kept refrigerated.

HiPCO® Single walled carbon nanotubes (purified, <15% wt% Fe impurities) were purchased from Unidym, Sunnyvale, CA and multi walled carbon nanotubes (95 + % C purity) from Nanocyl. Magnetic nanoparticles (Standard Carboxyl-Adembeads 0211 (100 nm) and master beads Carboxylic Acid 0215 (500 nm)) from Ademtech. Magnetic microparticles (Dynabeads M-270 carboxylic acid (2.4 μm)) were purchased from Invitrogen and carboxylated latex nanoparticles (100 nm) from Sigma.

β-Cyclodextrin modified glucose oxidase (GOX-CD) [17], mono-6-deoxy-6-amino-β-cyclodextrin [18], and mono-6-(2-pyrenebutylamino)-6-deoxy-β-cyclodextrin (pyrene-β-CD) [19] were synthesized as described in the corresponding references.

2.2. Apparatus

Electropolymerizations were performed in a conventional three-electrode cell, containing 0.1 mol L^{-1} phosphate buffer saline (PBS, mol L^{-1}, pH 7) as electrolyte solution with an Autolab potentiostat 100 (Eco Chemie, Utrecht, The Netherlands) using GPES software. An Ag/AgCl electrode was used as a reference electrode and a Pt wire, served as counter electrode.

Amperometric measurements for immunosensing on glassy carbon electrodes (Φ = 3 mm) were performed with an Autolab potentiostat 100 (Eco Chemie, Utrecht, The Netherlands) using GPES software, in stirred PBS (0.1 mol L^{-1} pH 7) containing the redox probe hydroquinone (2 mmol L^{-1}) at 25 °C by potentiostating the immunosensor at −0.1 V versus Ag/AgCl to detect enzymatically generated quinone.

The amperometric measurements for glucose sensor on Platinum electrodes (Φ = 2 mm) were performed with a Tacussel PRG-DL potentiostat (Tacussel, France) connected to a computer with E-recorder interface and controlled by the Echart software (eDAQ, Australia) in stirred PBS (0.1 mol L^{-1}, pH 7) at 25 °C by potentiostating the glucose sensor at 0.6 V versus Ag/AgCl to detect enzymatically generated H_2O_2.

FE-SEM images were recorded using ULTRA 55 FESEM 176 based on the GEMINI FESEM based on the GEMINI FESEM column with beam booster (Nanotechnology Systems Division, 178 Carl Zeiss NTS GmbH, Germany) and tungsten gun.

2.3. Preparation of amperometric immunosensors

The different 3D nanotube/nanoparticle scaffolds were used for amperometric immunosensors. The first layer of nanotubes (20 μL of 0.1 mg mL^{-1} in NMP) was deposited on glassy carbon (Φ = 3 mm) by classical drop casting [20]. Then, a nanoparticles suspension (5 μL of 0.5% volume) was deposited on top of the first SWCNT layer and dried under vacuum followed by washing with PBS. The second SWCNT layer was formed by depositing 10 μL (0.1 mg mL^{-1}) of nanotubes on the nanotube-nanoparticle assembly and dried as described earlier. These steps were applied using nanoparticles of different sizes (100 nm, 500 nm and 2.4 μm) to determine the appropriate pore size for the specific immunosensor application. Supplement levels were constructed by repeated deposition of nanotube (10 μL, 0.1 mg mL^{-1}) and nanoparticle (5 μL 0.5% volume) suspensions. The constructed scaffolds were then functionalized by incubating in a solution of pyrene-β-cyclodextrin (2 mmol L^{-1} in NMP). The pyrene layer was electropolymerized using cyclic voltammetry [21] by scanning between 0 and 1.3 V vs Ag/AgCl until the irreversible oxidation wave of pyrene disappeared (in average 2–3 scans).

The constructed scaffolds were characterized at each step with cyclic voltammetry (not shown) and SEM. For the immunosensors formation, the nanostructured working electrodes were incubated with biotinylated cholera toxin B subunit (10 μL, 0.5 mg mL^{-1}) dissolved in 1% (w/v) BSA/PBST for 20 min. After each step, the electrodes were rinsed with

0.1 mol L^{-1} PBS (pH 7) for several times. The immunosensors were incubated for 20 min with the analyte rabbit anti cholera toxin (anti-CT) antibody (10 μL) at concentrations ranging from 0.05 to 500 μg mL^{-1}. For labelling, a secondary antibody, horseradish peroxidase-labeled goat anti-rabbit IgG immunoglobulin (10 μL) at a concentration of 0.5 mg mL^{-1} dissolved in antibody diluent was deposited onto the sample exposed electrode for 20 min at 4 °C. The electrodes were then rinsed extensively with PBS. The HRP-immunosensor was potentiostated at −0.1 V versus Ag/AgCl in 10 mL stirred PBS containing the redox probe hydroquinone (2 mmol L^{-1}), to detect enzymatically generated quinone, in the presence of H_2O_2 (1 mmol L^{-1}). For glucose sensor, biotinylated glucose oxidase (GOx-B) (0.5 mg mL^{-1}, in PBS, 0.1 mol L^{-1}, pH 7.0, 20 min, 4 °C) was immobilized. All the experiments were repeated at least 3 times for each electrode and all the data were expressed as the mean ± standard deviation.

3. Results and discussion

3.1. *Scaffold construction*

The possibility of using iron catalyst impurities of HiPCO® produced SWCNTs as anchor points for magnetic nanoparticles, was first evaluated with magnetic carboxylated nanobeads (mNP) of an average diameter of 100 nm. A first SWCNT layer was formed by drop casting and drying of SWCNT dispersion in N-methyl pyrrolidone (NMP, 0.1 mg mL^{-1} in 20 μL). After deposition of the magnetic nanoparticles and subsequent rinsing, a relative homogeneous but not very dense layer of these nanoparticles was observed in the scanning electron microscopy (SEM) images (Fig. 1A).

To get further indications that the nanoparticles are principally retained via magnetic attraction, latex nanobeads (average diameter 100 nm) with the same surface functions (COOH) were drop cast on the SWCNT deposit. After applying identical treatments, only few individual particles or agglomerates could be identified on the SWCNT deposit (Fig. 1B).

After deposition of the next SWCNT layer, the resulting structures were examined using SEM. Fig. 2 shows the morphology of the surface and the cross-section of SWCNT-mNP-SWCNT layer and the randomly distributed mNP coated with a second SWCNT deposit. The cross-section of these first layers reveals that nanoparticles are covered by a thin film of web-like SWCNT deposit leaving as wanted some vacancies of up to several hundred nanometers.

These experiments were also performed using mNPs of 500 nm size and magnetic microbeads (~2.4 μm). Fig. 3 shows the SEM images of a double layer scaffold construction (SWCNT-mNP-SWCNT-mNP-SWCNT layer). Similarly, the top view of these deposits shows a web-like SWCNT layer on the top of both 100 nm and the 500 nm mNPs (Fig. 3A and B, respectively). The cross-section of these deposits reveals a more compact structure for the 100 nm nanoparticles whereas for the 500 nm nanoparticles, a recognizable LBL structure is visible.

In case of magnetic microbeads, some empty areas of the first SWCNT deposit were found. This might be due to the heavy weight of these particles and insufficient magnetic forces leading to rinsing off some of these microbeads during washing step. In addition, there was not a clear difference between single and double-layered structure.

After the structural characterization, the appropriateness of such SWCNT/nanoparticle of different sizes constructs was evaluated for immunosensing applications and compared with a conventional glucose biosensor.

3.2. *Anti-CT antibody detection using the HRP label secondary antibody for amperometric transduction*

To determine the most efficient scaffolds for anti-CT detection, all the LBL structures were compared to pure SWCNT deposits with an equivalent amount of nanotubes. The electrodes were prepared as described in the materials and methods section. Briefly, all structures were incubated in a pyrene-β-cyclodextrin (pyrene-β-CD) containing solution of (2 mmol L^{-1} in NMP) to form a thin pyrene coating throughout the nanotube/nanoparticle deposits [22]. Pyrene-β-CD was chosen since the pyrene groups form stable π-stacking interactions with the SWCNT sidewalls and the β-CD groups create a hydrophilic environment throughout the scaffold, enabling better diffusion of the biomacromolecules. Furthermore, β-CD forms stable inclusion complexes with biotin [23] which then allows the use commercialized biotinylated, antigen–antibody model immunosystems. To reinforce the formed

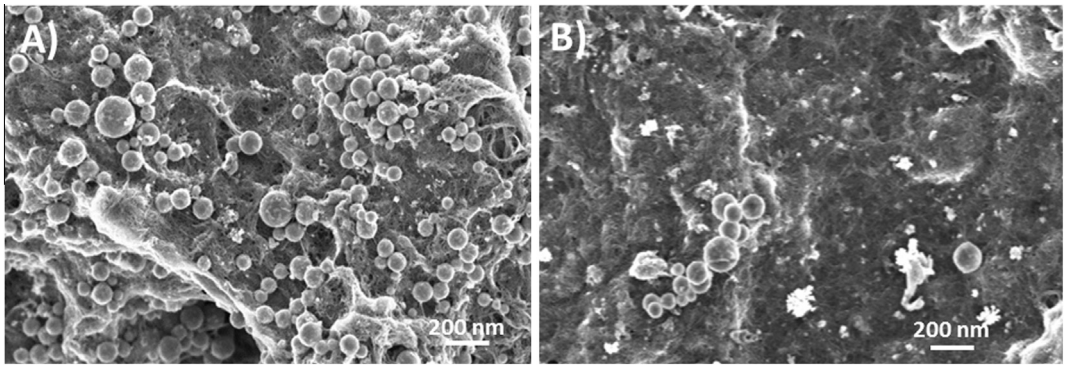

Fig. 1 – (A) Layer of mNP (100 nm) on the SWCNT deposit after rinsing. (B) Layer of latex nanoparticles (100 nm) on the SWCNT deposit after rinsing.

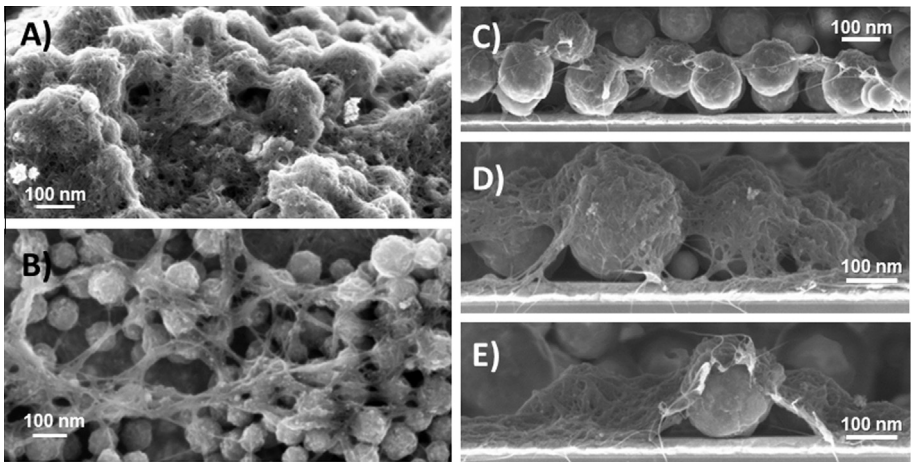

Fig. 2 – SEM images of (A and B) the topographic morphology of two representative areas of a SWCNT-mNP (100 nm)-SWCNT layer. (C, D, and E) are SEM images of the cross-section of these deposits.

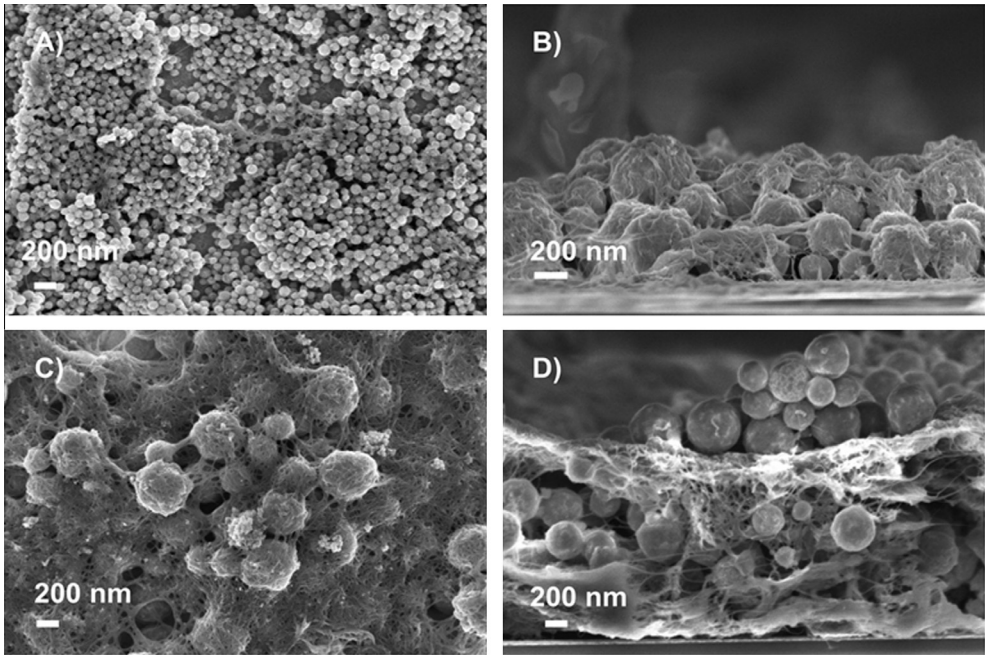

Fig. 3 – SEM images of (A) top view and (B) cross-section of a SWCNT-mNP (100 nm)-SWCNT-mNP (100 nm)-SWCNT deposit. (C) Topview and (D) cross-section of a SWCNT-mNP (500 nm)-SWCNT-mNP (500 nm)-SWCNT deposit.

construct, the attached pyrene groups were electropolymerized using cyclic voltammetry [21]. The "as prepared" electrodes were incubated with biotinylated cholera toxin B subunit to form the immunosensor. For optimal particle size determination, one analyte concentration (0.5 mg mL^{-1}) was used. After labelling with the horseradish peroxidase-tagged goat anti-rabbit IgG immunoglobulin, the maximum current densities of the different setups were determined by potentiostating the electrodes at −0.1 V vs Ag/AgCl in presence of hydroquinone (2 mmol L^{-1}) and 1 mmol L^{-1} of H_2O_2 [4]. Fig. 4 shows the histogram for the single and double layer structures formed with differently sized magnetic nano/microparticles and SWCNTs. As expected, there is a significant increase in immunosensor performance for nanostructures composed of nano/microparticles – nanotubes than for nanotubes only. The highest maximum current density (J_{max} = 117.14 ± 2.5 μA cm^{-2}) was recorded for 500 nm particles, clearly indicating the appropriateness of this construct arrangement for subsequent immobilization of the antigen, the analyte, and the HRP labelled secondary antibody. In contrast, the J_{max} value for the same amount of SWCNT without particles only reaches 41% of that observed for 500 nm particles (48.57 ± 0.8 μA cm^{-2}). The measured J_{max} also increased for the scaffold made of 100 nm particles and

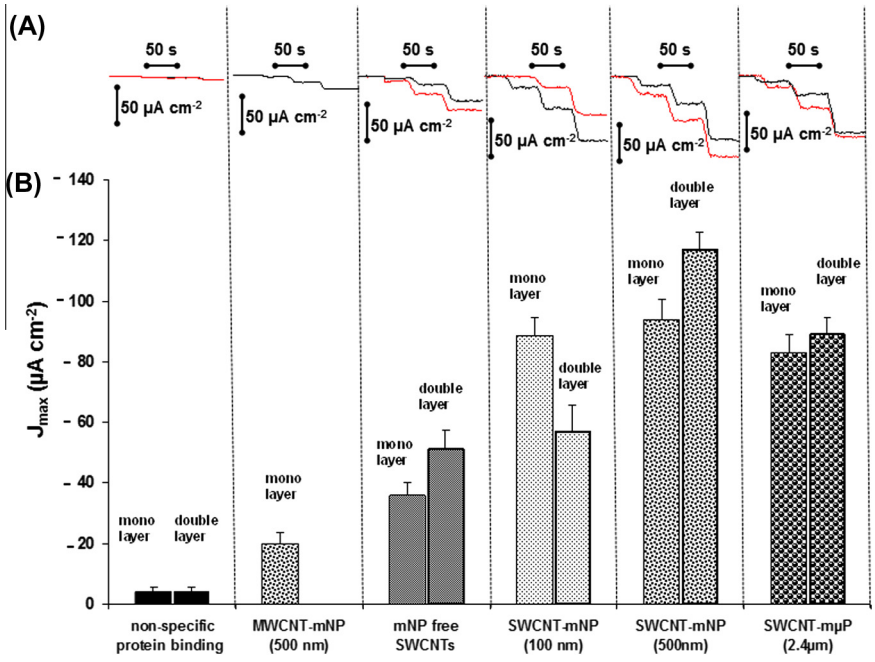

Fig. 4 – (A) Amperometric raw data recorded during H_2O_2 injections and (B) Histogram for initial evaluation of different configurations of mono- and double-layered nanostructured scaffolds using SWCNT, SWCNT and mNP (100 nm and 500 nm), and SWCNT/micro-beads (2.4 μm) along with control experiments for non-specific protein binding on poly(pyrene-β-CD) modified SWCNT-mNP scaffolds (HRP labelled secondary antibody without prior immobilization of the antigen receptor). The current densities were obtained after HRP labelling of the immobilized analyte with the secondary antibody (0.5 mg mL^{-1}) in PBS containing 2 mmol L^{-1} hydroquinone and 3 μmol L^{-1} of H_2O_2. The enzymatically generated quinone was reduced at −0.1 V vs Ag/AgCl. (A colour version of this figure can be viewed online.)

microbeads to reach 57.14 ± 0.9 μA cm^{-2} for 100 nm particles and 89.28 ± 2.7 μA cm^{-2} for microbeads (~2.4 μm), despite the inhomogeneity of the formed deposits.

The response time of all anti-CT immunosensors were considerably fast, ranging from 5 to 15 s. To confirm the beneficial role of magnetic attraction for the assembly of these structures, an additional control experiment using multi walled carbon nanotubes (MWCNTs) with 95% carbon purity and magnetic nanoparticles (500 nm) was done under identic conditions as for HiPCO® produced SWCNTs (Fig. 4) The maximum current density for MWCNTs – mNPs monolayer scaffolds of 20 ± 0.4 μA cm^{-2} was 6 times lower than that for HiPCO® SWCNTs constructions with the 500 nm mNPs. The combination of HiPCO® produced SWCNTs with its Fe impurities and magnetic nanoparticles of 500 nm size shows therefore to be the best configuration to construct such porous scaffolds for this immunosensor setup.

Moreover, to evaluate possible nonspecific binding of the secondary antibody and/or HRP on the modified nanotube surface, the poly(pyrene β-CD) modified nanotube/mNP (double layer, 500 nm mNPs) electrodes were incubated in PBS containing the HRP labelled secondary antibody. The obtained maximum current density of J_{max} = 4.3 μA cm^{-2} represents a general error of 3.6% compared to specific immune interactions. It has to be noted that this procedure has good reproducibility. The relative standard deviation (RSD) of three identically formed structures was 2.8% for 100 nm, 3.76% for 500 nm nanoparticles, and 5.46% for 2.4 μm microbeads.

3.3. *Anti-CT immunosensor performances using 500 nm particles*

To determine the sensitivity to anti CT, the immunosensors were constructed with 500 nm nanoparticles and SWCNTs, and tested with different concentrations of the target analyte (0.01–500 μg mL^{-1}). The calibration curve for the amperometric detection of CT antibody was evaluated for both, single and double-layered constructions. For each analyte concentration, an immunosensor was fabricated under same conditions. The sensitivities were determined as the slope of the linear portion of the calibration curves (Fig. 5). For single layered scaffold electrodes, a sensitivity of 77.55 ± 1.5 μA μg^{-1} mL cm^{-2} for the linear range between 0.05 and 0.2 μg mL^{-1} and a detection limit of 50 ng mL^{-1} could be determined. For the double-layered electrodes, the detection limit of 10 ng mL^{-1} is clearly improved and also a better sensitivity of 87.77 ± 2.2 μA μg^{-1} mL cm^{-2} for a linear range between 0.01 and 0.2 μg $mL^{-1}$is obtained. At lower antibody concentration, interferences with non-specifically bound HRP labelled secondary antibody appeared.

The detection limit, linear range, and sensitivity towards anti-CT are very satisfying compared literature. These performances are clearly higher than an equivalent 2D setup using amperometry [4], label-free electrochemical impedance spectroscopy [24], photoelectrochemical transduction [25], or nanomechanical detection techniques [26]. Only few examples report lower detection limits using high sophisticated

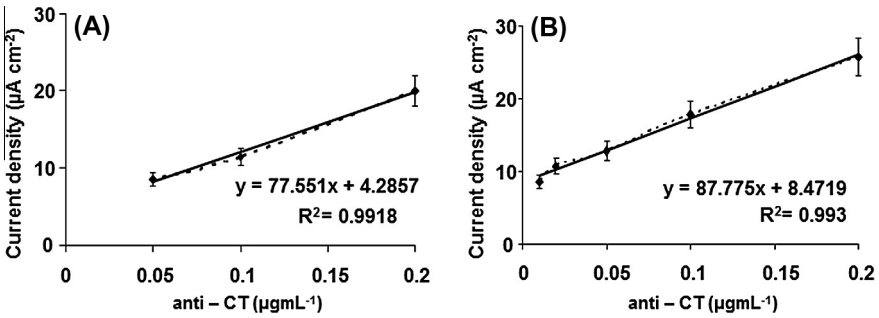

Fig. 5 – Linear range of the calibration curves for anti-CT with HRP-assisted amperometric transduction of (A) SWCNT – NP (500 nm) – SWCNT layer, and (B) SWCNT – NP (500 nm) – SWCNT – NP (500 nm) – SWCNT layer.

potential-step capacitance measurements [27] or nanocontainers with electroactive species, amplifying the electrochemical signal capture [28]. Nonetheless, targeted coating of the presented scaffold structures preventing the non-specific binding event still gives space for further improvements.

3.4. *Assessment of the scaffolds with different particle sizes for enzymatic glucose detection*

For comparison, the aforementioned constructions using different NP sizes were also used for enzymatic glucose biosensing. Biotinylated glucose oxidase (GOx-B) was immobilized on the nanotube – nanoparticle assembly and the resulting glucose sensor was calibrated with amperometric measurements. GOx catalyses the oxidation of glucose to gluconolactone by producing hydrogen peroxide out of oxygen. H_2O_2 is then oxidized at the Pt-electrode at 0.6 V versus Ag/AgCl, leading to current increase which is directly related to the glucose concentration.

The biosensor setup was constructed by depositing single and double layered structures of nanotubes and nanoparticles of different sizes on the Pt electrodes functionalized with pyrene-β-CD (as discussed earlier) and then used for the amperometric measurements. Fig. 6 presents the amperometrically recorded current changes and the histogram of recorded J_{max} values in presence of 70 mmol L^{-1} glucose.

For the enzymatic glucose sensor, 100 nm magnetic particles were found to be the most appropriate mNP size for the double-layer setup with an average maximum current density of 41.7 ± 0.7 μA cm^{-2}. By using the same procedure for scaffold construction, the maximum current density decreased with increasing particle size from 24.4 ± 0.5 μA cm^{-2} using 500 nm particles to 16.9 ± 0.5 μA cm^{-2} using 2.4 μm microbeads. This demonstrates the flexibility of the developed approach which can be adjusted and be optimized to the size of both the bioreceptor unit and the analyte (small molecules or biomacromolecules).

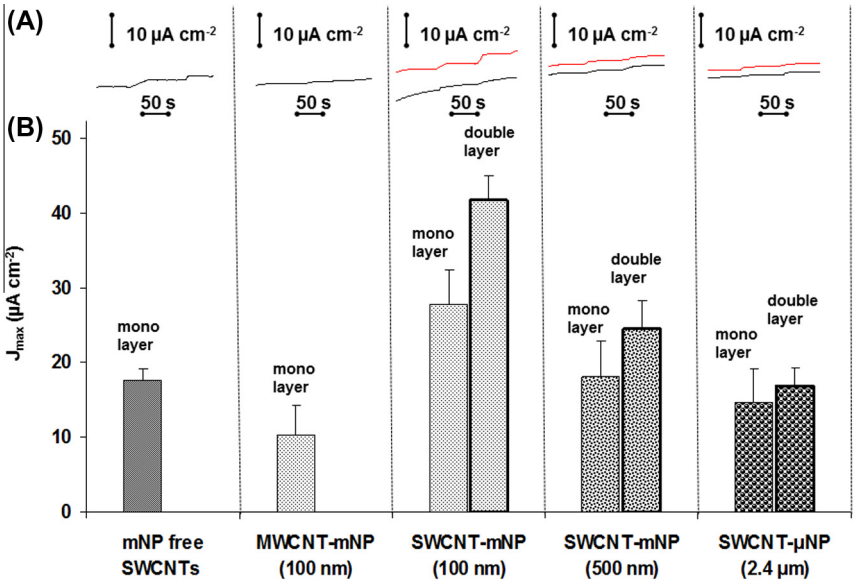

Fig. 6 – (A) Amperometric raw data recorded during glucose injections and (B) Histogram of the measured J_{max} values at 70 mmol L^{-1}containing glucose solution obtained with different mono-and double-layered scaffolds on Pt-electrodes using MWCNTs, SWCNTs, SWCNT/mNP (100 nm and 500 nm) and SWCNT/micro-beads (2.4 μm). The enzymatically generated H_2O_2 was oxidized at 0.6 V vs Ag/AgCl. (A colour version of this figure can be viewed online.)

Table 1 – Anti-CT immuno and glucose biosensor performances using different scaffold structures.

Particle size – layers	CNTs – mono layer	CNTs – double layer	100 nm – mono layer	100 nm – double layer	500 nm – mono layer	500 nm – double layer	2.4 μm – mono layer	2.4 μm – double layer
Immunosensor								
Current density: J_{max} (μA cm^{-2})	34.3	48.5	87.5	57.1	93.7	117.1	83.2	89.3
Sensitivity (μA L mol^{-1} cm^{-2})	–	–	–	–	77.5	87.8	–	–
Detection limit (ng L^{-1})	–	–	–	–	50	10	–	–
Glucose sensor								
Current density: J_{max} (μA cm^{-2})	–	17.6	27.8	41.7	18.1	24.4	14.6	16.9
Sensitivity (mA L mol^{-1} cm^{-2})	–	1.0	1.9	3	1.4	4.5	0.4	0.5

Control experiments were also conducted for this setup. By using only SWCNTs without mNPs, a maximum current density of 17.6 ± 0.3 μA cm^{-2} was obtained and using the MWCNT samples gave 10.5 ± 0.4 μA cm^{-2}. Compared to these values, the increase of the configuration using the 100 nm mNPs is not that impressive as for the immunosensing experiments. It seems that for enzyme biosensors smaller nanoparticle sizes are more appropriate for clearer performance increases. Nonetheless, a convincing reproducibility was also obtained for this setup with RSDs of 1.7% for 100 nm, 2.2% for 500 nm nanoparticles, and 2.9% for 2.4 μm microbeads, evaluating three identically formed structures.

Significant features of the immunosensor and the glucose biosensor are summarized in Table 1.

4. Summary

3D nanostructured scaffolds made with "as received" commercial HiPCO® SWCNTs and magnetic nanoparticles (mNPs) with different sizes were constructed on transducer surfaces using a simple LBL process for high performance immunosensors. The iron nanoparticle impurity in HiPCO® SWCNTs was used as anchor points to retain randomly mNPs. The proof of concept for their application in biosensing has been shown by enzymatic glucose detection. While both, monolayer and double layer scaffolds containing 100 nm particles were found to meet the desirable sensitivity for this enzyme biosensors, scaffolds embedding 500 nm mNPs, presented the highest anti-CT immunosensors performance compared to other constructions using either smaller or bigger particle sizes. Therefore, the vacancies created with 500 nm mNPs seem to present the most suitable pore size for the permeation of the analyte and for HRP labelled secondary antibody. By using the nanoparticle size of 500 nm, a detection limit of 10 ng mL^{-1} and a sensitivity of 87.77 μA μg^{-1} mL cm^{-2} towards anti-CT could be reached. Except few examples described above, this is by far the highest sensitivity for anti-CT immunosensors compared to equivalent setups using amperometric transduction [4] or ELISA used for clinical analysis [29]. It has to be noted that the used commercialized mNPs are polydisperse with average particle sizes. Together with the inhomogeneous deposition of the mNPs on SWCNTs, pore sizes from several nanometers to several micrometers were observed. This allows unhindered diffusion of all biomolecules throughout the structure to the more densely packed anchor groups and receptor units. Nonetheless, these randomly assembled structures shows as a whole good reproducibility for all evaluated setups. The approach developed within this work, one can therefore take advantages of the presented proof of concept for these scaffolds construction in order to customize the pore sizes for any type of bioanalytical or bioenergy devices just by choosing the most appropriate mNP size.

Acknowledgment

The authors would like to thank the platform 'functionalization of surfaces and transduction' of the scientific structure 'Nanobio' for providing facilities, Dr. Jessica Baur for initial

tests, and Arielle Le Pellec for assistance. The authors would also like to thank the French–Canadian Research Found (FCRF) for the Ph.D fellowship for MS. The present work was partially supported by the Labex ARCANE (ANR-11-LABX-0003-01).

REFERENCES

[1] Walcarius A, Minteer SD, Wang J, Lin Y, Merkoci A. Nanomaterials for bio-functionalized electrodes: recent trends. J Mater Chem B 2013;1(38):4878–908.
[2] Dai Z, Ju H. Bioanalysis based on nanoporous materials. TrAC – Trends Anal Chem 2012;39:149–62.
[3] Marquette CA, Blum LJ. State of the art and recent advances in immunoanalytical systems. Biosens Bioelectron 2006;21(8):1424–33.
[4] Ionescu RE, Gondran C, Cosnier S, Gheber LA, Marks RS. Comparison between the performances of amperometric immunosensors for cholera antitoxin based on three enzyme markers. Talanta 2005;66(1):15–20.
[5] Ju H, Zhang X, Wang J. Nanomaterials for Immunosensors and Immunoassays. In: NanoBiosensing. Springer: New York; 2011. p. 425–52.
[6] Wang J. Carbon-nanotube based electrochemical biosensors: a review. Electroanalysis 2005;17(1):7–14.
[7] Chen RJ, Choi HC, Bangsaruntip S, Yenilmez E, Tang X, Wang Q, et al. An investigation of the mechanisms of electronic sensing of protein adsorption on carbon nanotube devices. J Am Chem Soc 2004;126(5):1563–8.
[8] Le Goff A, Holzinger M, Cosnier S. Enzymatic biosensors based on SWCNT-conducting polymer electrodes. Analyst 2011;136(7):1279–87.
[9] Holzinger M, Haddad R, Maaref A, Cosnier S. Amperometric biosensors based on biotinlylated single-walled carbon nanotubes. J Nanosci Nanotechnol 2009;9(10):6042–6.
[10] Haddad R, Cosnier S, Maaref A, Holzinger M. Non-covalent biofunctionalization of single-walled carbon nanotubes via biotin attachment by π-stacking interactions and pyrrole polymerization. Analyst 2009;134:2412–8.
[11] Chen Y, Iqbal Z, Mitra S. Microwave-induced controlled purification of single-walled carbon nanotubes without sidewall functionalization. Adv Funct Mater 2007;17(18):3946–51.
[12] Chiang IW, Brinson BE, Huang AY, Willis PA, Bronikowski MJ, Margrave JL, et al. Purification and characterization of single-wall carbon nanotubes (SWNTs) obtained from the gas-phase decomposition of CO (HiPco process). J Phys Chem B 2001;105(35):8297–301.
[13] Georgakilas V, Voulgaris D, Vazquez E, Prato M, Guldi DM, Kukovecz A, et al. Purification of HiPCO carbon nanotubes via organic functionalization. J Am Chem Soc 2002;124(48):14318–9.
[14] Vazquez E, Georgakilas V, Prato M. Microwave-assisted purification of HIPCO carbon nanotubes. Chem Commun 2002;20:2308–9.
[15] Wiltshire JG, Khlobystov AN, Li LJ, Lyapin SG, Briggs GAD, Nicholas RJ. Comparative studies on acid and thermal based selective purification of HiPCO produced single-walled carbon nanotubes. Chem Phys Lett 2004;386(4–6):239–43.
[16] Bittova B, Vejpravova JP, Kalbac M, Burianova S, Mantlikova A, Danis S, et al. Magnetic properties of iron catalyst particles in HiPco single wall carbon nanotubes. J Phys Chem C 2011;115(35):17303–9.
[17] Holzinger M, Bouffier L, Villalonga R, Cosnier S. Adamantane/β-cyclodextrin affinity biosensors based on single-walled carbon nanotubes. Biosens Bioelectron 2009;24(5):1128–34.
[18] Hamasaki K, Ikeda H, Nakamura A, Ueno A, Toda F, Suzuki I, et al. Fluorescent sensors of molecular recognition. Modified cyclodextrins capable of exhibiting guest-responsive twisted intramolecular charge transfer fluorescence. J Am Chem Soc 1993;115:5035–40.
[19] Ogoshi T, Takashima Y, Yamaguchi H, Harada A. Chemically-responsive sol–gel transition of supramolecular single-walled carbon nanotubes (SWNTs) hydrogel made by hybrids of SWNTs and cyclodextrins. J Am Chem Soc 2007;129(16):4878–9.
[20] Haddad R, Cosnier S, Maaref A, Holzinger M. Electrochemical characterization of biotin functionalized and regular single-walled carbon nanotube coatings. Application to amperometric glucose biosensors. Sensor Lett 2009;7(5):801–5.
[21] Haddad R, Holzinger M, Maaref A, Cosnier S. Pyrene functionalized single-walled carbon nanotubes as precursors for high performance biosensors. Electrochim Acta 2010;55(27):7800–3.
[22] Haddad R, Holzinger M, Villalonga R, Neumann A, Roots J, Maaref A, et al. Pyrene-adamantane-β-cyclodextrin: an efficient host-guest system for the biofunctionnalization of SWCNT electrodes. Carbon 2011;49:2571–8.
[23] Holzinger M, Singh M, Cosnier S. Biotin-β-cyclodextrin: a new host-guest system for the immobilization of biomolecules. Langmuir 2012;28(34):12569–74.
[24] Haddour N, Chauvin J, Gondran C, Cosnier S. Photoelectrochemical immunosensor for label-free detection and quantification of anti-cholera toxin antibody. J Am Chem Soc 2006;128(30):9693–8.
[25] Yao W, Le Goff A, Spinelli N, Holzinger M, Diao G-W, Shan D, et al. Electrogenerated trisbipyridyl Ru(II)-/nitrilotriacetic-polypyrene copolymer for the easy fabrication of label-free photoelectrochemical immunosensor and aptasensor. Application to the determination of thrombin and anti-cholera toxin antibody. Biosens Bioelectron 2013;42:556–62.
[26] Soo-Hyun T, Aditi D, Stephen S, Vinayak PD. Nanomechanical detection of cholera toxin using microcantilevers functionalized with ganglioside nanodiscs. Nanotechnology 2010;21(43):435–502.
[27] Loyprasert S, Hedström M, Thavarungkul P, Kanatharana P, Mattiasson B. Sub-attomolar detection of cholera toxin using a label-free capacitive immunosensor. Biosens Bioelectron 2010;25(8):1977–83.
[28] Viswanathan S, Wu L-c, Huang M-R, Ho J-aA. Electrochemical immunosensor for cholera toxin using liposomes and poly(3,4-ethylenedioxythiophene)-coated carbon nanotubes. Anal Chem 2006;78(4):1115–21.
[29] Leshem B, Sarfati G, Novoa A, Breslav I, Marks RS. Photochemical attachment of biomolecules onto fibre-optics for construction of a chemiluminescent immunosensor. Luminescence 2004;19(2):69–77.